# Soft Growing Pin for High-Extension Shape-Changing Displays

Antonio Alvarez Valdivia<sup>1</sup>, Mohammad A. Rezqalla<sup>1</sup>, Sarah E. Swann<sup>1</sup>, Laura H. Blumenschein<sup>1</sup>

Abstract—Regular user interface screens can display dense and detailed information to human users but miss out on providing somatosensory stimuli that take full advantage of human spatial cognition. Therefore, the development of new haptic displays can strengthen human-machine communication by augmenting visual communication with tactile stimulation needed to transform information from digital to spatial/physical environments. Shape-changing interfaces, such as pin arrays and robotic surfaces, are one method for providing this spatial dimension of feedback; however, these displays are often either limited in maximum extension or require bulky mechanical components. In this paper, we present a compact pneumatically actuated soft growing pin for inflatable haptic interfaces. Each pin consists of a rigid, air-tight chamber, an inflatable fabric pin, and a passive spring-actuated reel mechanism. The device behavior was experimentally characterized, showing extension to 18.5 cm with relatively low pressure input (1.75 psi, 12.01 kPa), and the behavior was compared to the mathematical model of soft growing robots. The results showed that the extension of the soft pin can be accurately modeled and controlled using pressure as input. Finally, we demonstrate the feasibility of implementing individually actuated soft growing pins to create an inflatable haptic surface.

## I. INTRODUCTION

Human-computer interactions are becoming more ubiquitous as smart devices are introduced into human environments. These new applications of technology bring the need for new interaction modalities; shape-changing interfaces present one option to fundamentally shift how humans and computers interact, as humans can physically interact with information while it is manipulated in space [1]-[3]. Many current shape changing displays use grids of extending pins to move a 2D grid into 3D space. These "2.5D" pin-displays can render a variety of distinguishable shapes with high surface extension and fast actuation speed [4]–[8], with some achieving human-scale shape rendering [9], [10]. One major challenge in developing rigid pin displays has been reducing the bulky enclosures necessary to store the actuators and the pins when not extended. These factors limit the portability of shape-changing displays, and suggests that compliant and elastic materials may be necessary to achieve the large desired change in volume. Separately, there have also been calls to investigate compliant materials for their potential to produce new sensations and interactions [1].

Current work in compliant shape-changing interfaces has yielded designs for a range of applications, such as soft interfaces for programmable surfaces [11], [12], refreshable braille displays [13] and soft skin texture modulation [14].

This work is supported in part by the NSF Graduate Research Fellowship Program (DGE-1842166) and by NSF Grants #2129201 and #2129155.

<sup>1</sup>School of Mechanical Engineering, Purdue University, West Lafayette, IN 47901 USA (e-mail: alvar168@purdue.edu; lhblumen@purdue.edu)

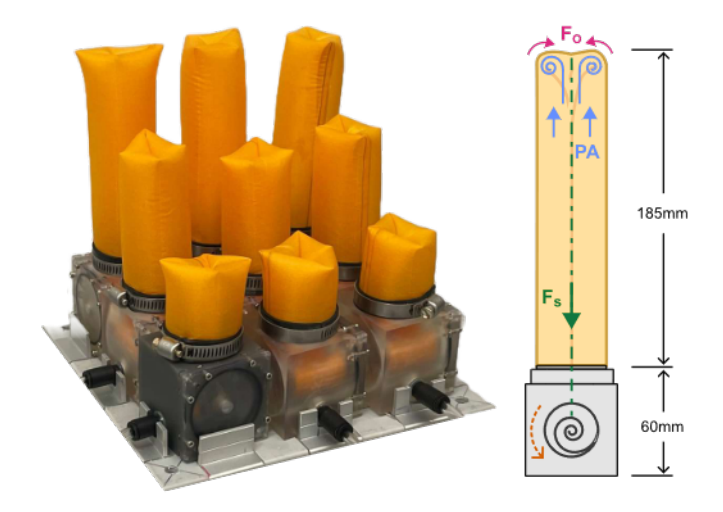


Fig. 1. The soft growing pin is a compact pneumatically actuated device capable of extending 308% relative to the size of the pin at its initial state. We demonstrate the feasibility of implementing these pins to create inflatable shape-changing displays.

This work has also led to new behaviors not achievable with rigid pin displays; particle jamming soft robotic displays can create surface stiffness change using vacuum, allowing these displays to render multiple geometries and adjust surface mechanical properties [15]. Mixed soft-rigid displays, such as inflatable 3D texture-morphing surfaces [16], impedance-style haptic terrain displays [17], soft robotic surfaces for regulating environmental perceptions [18], [19], and programmable shape changing displays with electroadhesive auxetic skins and pneumatic actuation [20], provide a middle-ground on the advantages of soft vs. rigid surfaces. However, the addition of compliant material alone has not solved the higher extension need; displays using elastic material often still have small total extension [13].

One recent approach to high extension pins displays has been to create retractable pins which can be flattened and stored on a reel inside compact, individual housings. Bistable sheets like those found in tape measures [21] have been used for table-top, shape-changing haptic devices and pneumatically inflated high-extension actuation for 3D robotic structures [22]. These designs attain high extension, but can become impeded by the environment or other pins as the full pin needs to move to continue extending and the low stiffness of the pin makes it prone to buckling. In the past decade, a new class of robots that "grow" via pressure-driven eversion has emerged [23]. Growing soft robots extend by adding material at the tip instead of the base; the new material initially travels within the robot's body so its movement is not impeded by the environment [24], [25]. However, pressure can only cause robot extension, creating the need for additional devices to provide retraction [26]. Here we propose to develop a pneumatically driven pin using extension by growth with a passive return.

Inspired by recent developments on shape-changing pin displays and soft growing robots, this work presents a soft, flexible growing pin for shape-changing inflatable displays with high extension (308%) and passive retraction (Figure 1). Section II introduces the concept behind the growing pin and the theoretical force balance to control the extension. Section III then describe the design and construction of the growing pin followed by characterization of the behavior in Section IV. Finally, Section V demonstrates a 9-pin openloop controllable pin display using growing pins. The work ends with a discussion of the design and modeling results.

#### II. SOFT GROWING PIN CONCEPT

In this section, we will describe each of the growing pin components. We also review and expand the mechanical model of growing robots to account for passive retraction.

## A. Inherent Components and Working Principles

The soft-growing pin display concept consists of three components: 1) a pressure tight growing body for the pin, 2) a mechanism to retract the pin, and 3) a vessel to contain these components. This composition builds on previous growing robot designs with two modifications [27]: i) scaling the growing robot and ii) using a passive retraction mechanism. Scaling down the growing robot tube allows for a greater "resolution" of 3D reconstructions. The footprint of the base vessel for the pin should be scaled to be equal to the pin diameter, allowing tighter packing and less distance between pins. The second modification, the passive retraction, serves to help scale down the vessel footprint. In previous growing robot designs, retraction was achieved through motors at the base or tip, increasing the vessel size or preventing vertical growth. With a passive retraction mechanism, as the pin is pressurized, the growing body will extend due to the pressure force, balanced by the force of the passive retraction mechanism.

# B. Mechanical Modeling

Given the working principle of the soft growing pin, its behavior can be derived from combining models of growing robot mechanics and knowledge of the passive retraction force. The mathematical model that describes pressure driven eversion, i.e. the relationship between growth and pressure for a growing robot [24], [26], accounts for how the pressure puts both the internal and external material into tension. An offset,  $F_o$ , develops between the internal and external wall tensions, which results in a minimum pressure to grow or force to retract. For the soft growing pin, the tension in the tail (i.e. the internal material) is represented by  $F_T$  where:

$$F_T = \frac{1}{2}PA \pm F_o \tag{1}$$

where P is the applied pressure, A is the cross-sectional area of the body, and  $F_o$  is the force loss that causes the tension offset. With passive retraction, the tension in the tail

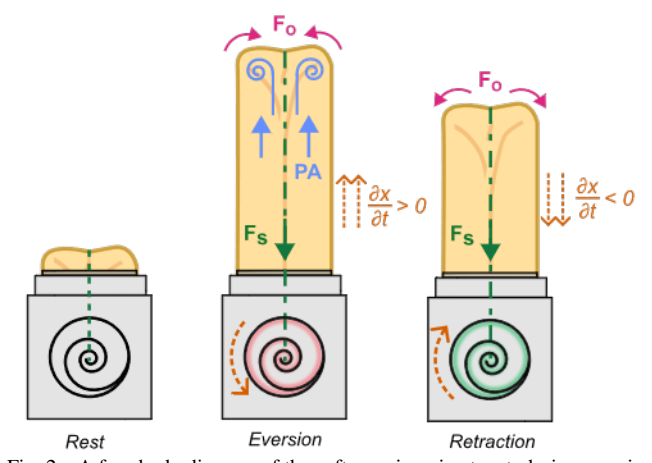


Fig. 2. A free-body diagram of the soft growing pin at rest, during eversion, and during retraction. When pressure P is applied, the tension in the spring  $F_S$  increases as the growing body everts. In retraction, as the pressure decreases so does the spring tension.  $F_o$  represents frictional force losses that offset the tension in extension and retraction.

 $F_T$ , can be replaced by the force of the passive mechanism,  $F_S(x, \frac{\delta x}{\delta t})$ . This force can be empirically determined as a function of the current pin length, x, and the current direction of growth velocity  $\frac{\delta x}{\delta t}$ . This function will be described further in Section IV-C. Figure 2 provides an overview of these variables in the force balance. Since the pressurized air is the driver of growth, we solve for the pressure needed to reach a certain length x:

$$P = \begin{cases} \frac{2}{A} (F_S(x, \frac{\delta x}{\delta t}) - F_o) & \frac{\delta x}{\delta t} < 0\\ \frac{2}{A} (F_S(x, \frac{\delta x}{\delta t}) + F_o) & \frac{\delta x}{\delta t} > 0 \end{cases}$$
(2)

Given this model, the pin's growth can theoretically be controlled by the pressure, if both the behavior of the passive retraction mechanism,  $F_S$ , and the force loss from growth,  $F_o$ , are known. Additionally, these equations suggest that  $F_S$  must remain greater than  $F_o$  during retraction, otherwise a negative pressure will be predicted.

#### III. DEVICE CONSTRUCTION

The soft growing pins were constructed with relatively inexpensive components and with a range of springs tested as the retraction mechanism (Figure 3). All 3D printed parts were manufactured with a Form 3+ Formlabs resin printer.

The growing body is made of 1.3 oz, 30-denier silicone impregnated ripstop fabric (FRC13, Seattle Fabrics). The fabric shows low self friction when layers of the fabric may interfere with each other when folded, reducing the overall force loss from growth. The growing body is manufactured by hand; first, the fabric is cut following the planar outline of a cylinder with a diameter of 1.5 in (3.81 cm) and 25 in (63.5 cm) in length. The overhang edges are bonded using a lap joint with a silicon epoxy (Sil-poxy, Smooth-On) forming a tube. One end of the growing body is sealed with silicon epoxy and the growing body is folded in half axially in order to fit the width of the vessel. The sealed end is then affixed to a reel with double-sided viscoelastic tape (MD9000, Marker-Tape), and the body is wound around the reel to be installed in the vessel. An o-ring is installed on a groove located in the outside of the vessel opening and then the free end of the

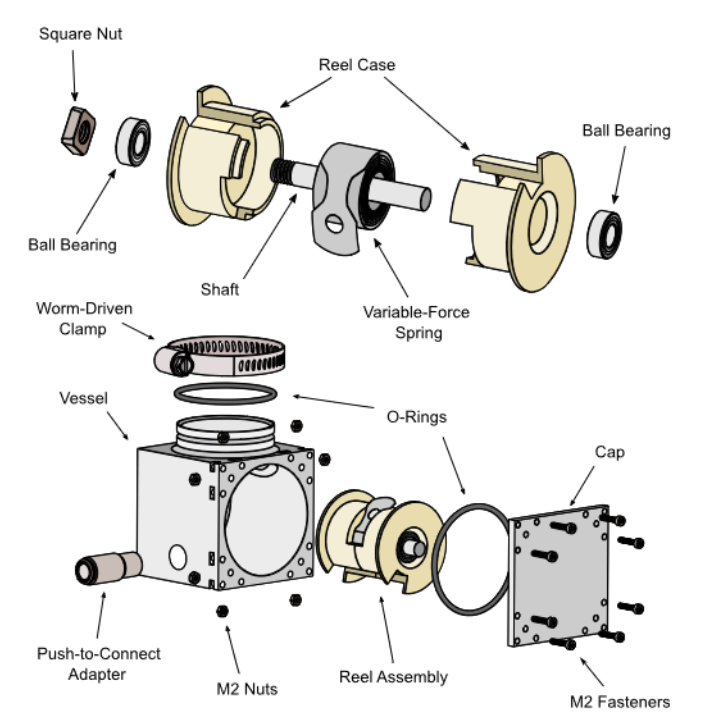


Fig. 3. (Top) Spring-actuated reel assembly. The spring is machined to feature a keyed end that is placed in a gap/aperture in the case to secure it to the case. The other end is mechanically attached to the shaft with a retaining screw. (Bottom) Full soft growing pin assembly. The growing body (not shown) is installed on the vessel opening and secured in place by the worm-driven clamp.

growing body is pulled through the opening, turned inside out, and then placed over the o-ring. Finally the growing body is secured firmly by a worm-driven clamp (5388K26, McMaster-Carr) placed over a rubber strip to protect the fabric.

The reel where the growing body is wound-up is also the location of the retraction mechanism. The spring-actuated reel is designed to allow efficient retraction of the growing robot with simple, low-cost components. The reel is made of a torsion spring encased in a rotating case. The reel assembly (shown in Figure 3) is made up of a shaft, a torsion spring, bearings, and a 3D printed housing. The springs were selected from standard catalog-ready springs (McMaster-Carr). Four different springs were tested: two with constant-force and two with variable-force.

One end of the spring was mechanically held in place with a retaining screw to a 6 mm aluminum shaft. Around this shaft a 3D printed case acted as both the reel for the material and a housing for the spring. The case was divided into segments to facilitate assembly and insertion of the other components. Ball bearings (7804K112, McMaster-Carr) are placed on each end of the housing segments. The shaft and spring subassembly is then placed in between the two housing segments and through the bearings. As shown in Figure 3, the spring is encased inside the reel case; the loose end of the spring was machined to feature a keyed end that is placed in a case gap/aperture to secure the spring to the case. The case segments are then glued or taped together. To finish the reel assembly, a square nut (97258A104, McMaster-Carr) is screwed into the threaded end of the shaft and Loctite is

applied to lock it in place.

The reel assembly with growing body is placed into the air-tight vessel to complete the assembly. The vessel is a 3D printed part shaped as a 2 in (5.08 cm) cube with a hollow cylindrical opening for the reel. The vessel features an inlet for pressurized air input, where a push-to-connect adapter (5779K718, McMaster Carr) is glued in place using adhesive epoxy (DP110, 3M). On the inner wall opposite to the open end of the vessel, there is a square-shaped hole to secure the shaft assembly, retaining alignment and stopping rotation. Since the shaft is locked in place, the only component free to rotate is the reel housing, which internally transmits the mechanical rotation to the spring. The vessel is sealed with a 3D printed end cap using M2 fasteners and nuts. The cap has an internal guide hole to align the shaft assembly and an o-ring to ensure air-tightness.

## IV. DEVICE CHARACTERIZATION

To validate and fit our theoretical model of a soft growing pin with passive retraction mechanism (Section II), we performed a series of experiments on the components and full system to measure the relationships between pressure, pin length, and internal tension force.

## A. Characterizing Pressure vs. Extension

Four different reels were constructed, each featuring a distinct spring (with constant or variable force). Table I shows the nominal force ratings and lengths of the springs. Since it is expected that the spring behavior will significantly effect the retraction of the pin, we first tested each spring in the full assembly, observing its behavior when pressurized.

For this experiment, the growing pins were pressurized and depressurized to observe the quasi-static pressure-length relationship. A time-of-flight (ToF) sensor (VL53L1X, CQRobot) was placed 50 cm above the growing pin when fully retracted to measure the extension of the device. Due to the relatively translucent nature of the fabric, a rigid lightweight cap (7 g) was placed on the tip of the soft growing pin to provide a consistent surface for the sensor to measure [27]. The pressurized air supply consisted of a pressure regulator with built-in exhaust (QB3, Proportion Air) and an external electronic pressure sensor (015PGAA5, Honeywell Sensing). The pressure regulator was controlled and interfaced to the pressure sensor and the ToF sensor using an Arduino Uno.

The experiments began completely unpressurized. Pressure was increased in steps of 0.1 psi (0.69 kPa), up to a maximum extension, defined as the third consecutive pressure step at which the pin length no longer changed. For the growing pins tested, this maximum extension generally happened around 2 psi (13.79 kPa); after reaching this maximum pressure, decrement steps of 0.1 psi (0.69 kPa) were performed until the fully unpressurized state was reached. In between each increment or decrement, a pause was taken to allow the pin to reach a quasi-static state. Sensor measurements were analyzed off-line using MATLAB. This experimental procedure was repeated for each spring-actuated reel.

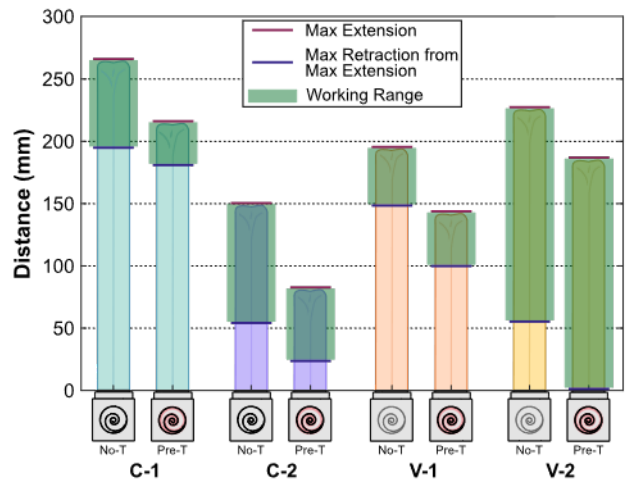


Fig. 4. Experimental characterization of Pressure vs. Extension. The eight spring variations were tested. Only the second variable force spring (V-2) with pretension was capable of fully retracting, reaching a maximum height of 18.5 cm, representing a 308% length change relative to the size of the soft growing pin at its initial state.

The results of these experiments are summarized in Table I and Figure 4. Initially, all the reels were tested without pretension in the springs. As observed in Figure 4, without pretension, no reel was capable of fully retracting the growing body. In other words, after reaching full extension and starting to decrease pressure, the pins would reach a point at which they would not retract anymore. This behavior effectively shortened the working range of the pins to just a portion of their maximum extension. With this observation, we tested each spring pre-tensioned by one full turn. This gives the eight tested configurations, with only the second variable force spring with pretension (V-2) capable of fully retracting. This spring reached a maximum height of 18.5 cm, or a length change of 308% relative to the initial size of the soft growing pin (Table I). Full length to pressure characterization for this configuration is shown in Figure 5.A, showing the large hysteresis between growth and retraction.

Looking at the full results over spring type and pre-tension level, the spring type and condition offered interesting trade-offs. On the one hand, pre-tensioning the springs universally lowered the maximum extension of each of the reels, since the reel essentially had one fewer turn to allow the pin to grow. On the other hand, as expected, pretension of the pin improved retraction by keeping the spring force  $(F_S)$  above the force loss of eversion  $(F_o)$  for longer. In most cases, this did not end up improving the working range overall, because of the lower total extension. Again, only the variable force spring V-2 accessed 100% of the working range. Given this, the remaining experimental characterization was performed on this *best case* prototype.

## B. Characterizing Spring Force vs. Extension

Continuing the characterization, we examine the force length relationship of the spring in the reel alone, i.e.  $F_S(x,\frac{dx}{dt})$ . For this experiment, the reels were placed on the base of a vertical force-strain test stand (ESM303, Mark-10). A force gauge (M7-100, Mark-10) was used to measure the force of the spring as the test stand pulled on the reel

Spring	Force	Length	Pin Max. Extension (%)	
Type	(N)	(m)	No Pre-Tension	Pre-Tension
C-1	2.94	0.38	440.00	356.67
C-2	5.47	0.31	248.33	135.00
V-1	0 - 4.45	0.56	323.33	236.67
V-2	0 - 5.40	0.36	376.67	308.33

TABLE I

NOMINAL CHARACTERISTICS AND PERFORMANCE OF TESTED SPRINGS.

up to the instrument's maximum extension of 280 mm at a rate of 330 mm/min, and then back down to the initial state. To relate this test stand height to the equivalent pin height, we divide by two. This is because the pin's growing body only extends halfway along the linear extension tangential to the reel rotation. Therefore, the maximum extension tested was equivalently 140 mm of pin extension (Figure 5.B). The force gauge tension and encoder readings were transmitted to a computer with serial communication. The fabric growing body on the reel was replaced by non-stretch nylon cord, allowing for more accurate readings of the tension vs. extension relationship of the spring. The results of this experiment (Figure 5) shed more light on the full pin behavior. During extension, the reel shows a (relatively) linear increase in tension as the length increases. However, once the length starts decreasing, there is a drastic drop of the spring force, demonstrating a major source of the observed hysteresis in Figure 5.

## C. Characterizing Internal Tension vs. Pressure

The last experiment measured the offset force imposed by the material eversion,  $F_o$ . To measure for frictional losses and material effects associated with the growing body, we used a motorized growing robot base to observe the P vs.  $F_T$  relationship [26]. The growing robot base is composed of a pressure tight drum and spool with a geared DC motor and encoder that enables controlled growth and retraction. The base features a tension transducer (LCM100, Futek) that directly measures  $F_T$ .

The soft growing pin body was mounted on the growing robot base. The chamber pressure is increased to a setpoint and, once this pressure is reached, the system allows the body to start growth. When a predetermined length is reached, the system retracts the body. During this eversion-retraction cycle, the tension transducer measures the internal tension. Off-line data processing in MATLAB separates the measurements for eversion and retraction in each cycle. After filtering the data, the analysis processes mean and standard deviations for eversion and retraction at each pressure P. This experimental process was repeated for six pressure values from 0 to 1.75 psi.

The results of these experiments are shown in Figure 6, with the offset of the data from the line  $F=\frac{1}{2}PA$  representing  $F_o$ , measured as 0.13 N for eversion, and 0.37 N for retraction. To compare to this more direct measurement of  $F_o$ , we calculate the value of  $F_o$  predicted by the pressure versus pin length and tension versus spring extension data (Figure 5). For each length, x, of the pin, we find the corresponding tension force,  $F_S(x,\frac{\delta x}{\delta t})$ , produced by the spring and plug the values in to Equation 2 to solve for

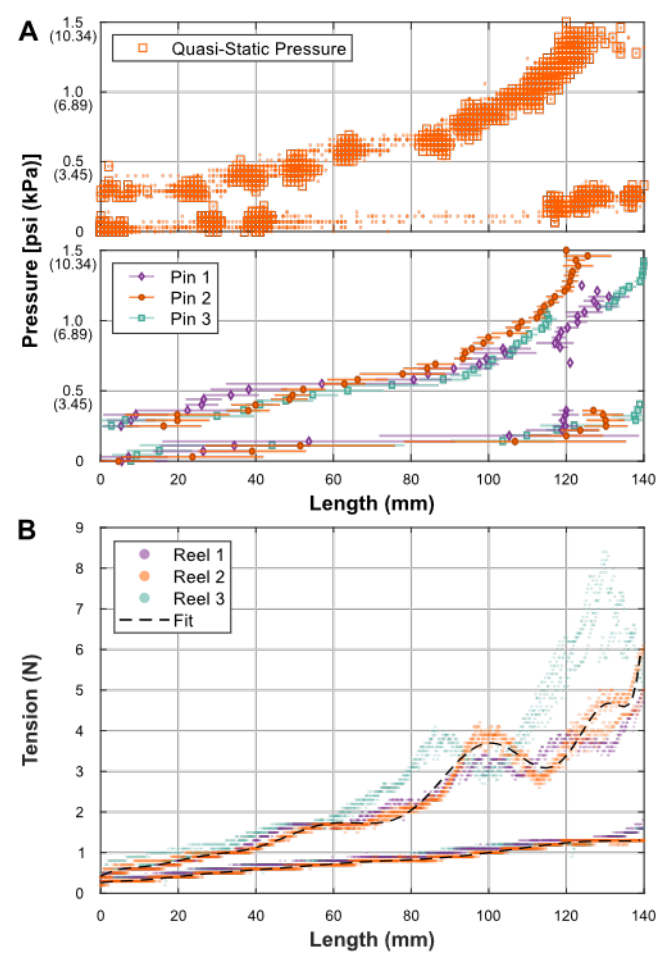


Fig. 5. Experimental characterization of three growing pins using the best-performing pin model (V-2 with pre-tension). (A) Length to Pressure characterization. Quasi-static states were considered to characterize the behavior. The mean and standard deviation of experimental data for the three pins exhibit show some variation in growth rates. (B) Length to Tension characterization. Variations in the reel behavior may account for the observed differences in growth rates in (A). In both (A) and (B) plots we can observe significant hysteresis between growth and retraction.

the value of  $F_o$  alone. To test whether the behavior matches previous models of vine robots, the best estimate of  $F_o$ , fit separately for extension and retraction, is shown by the fit line with slope A/2 (Figure 6). This value, defined as the intercept of the fit line with the y-axis, was found to be 0.58 N for eversion, and 0.28 N for retraction. The close agreement between the direct measurement and calculated value indicate that the pin behavior is well described by a combination of the material eversion force and spring force and that the major source of hysteresis in the pin behavior can be explained by the spring hysteresis alone.

# V. DEMONSTRATION

To demonstrate the feasibility of implementing the soft growing pins to create surface displays, we conducted an experimental demonstration with a 3x3 array of individually actuated units. Said demonstrations enabled a comprehensive exploration of the capabilities of the soft growing pins.

The setup consists of nine soft growing pins arranged as a 3x3 array. A structural frame was constructed using aluminum extrusions and interconnected using press-fit con-

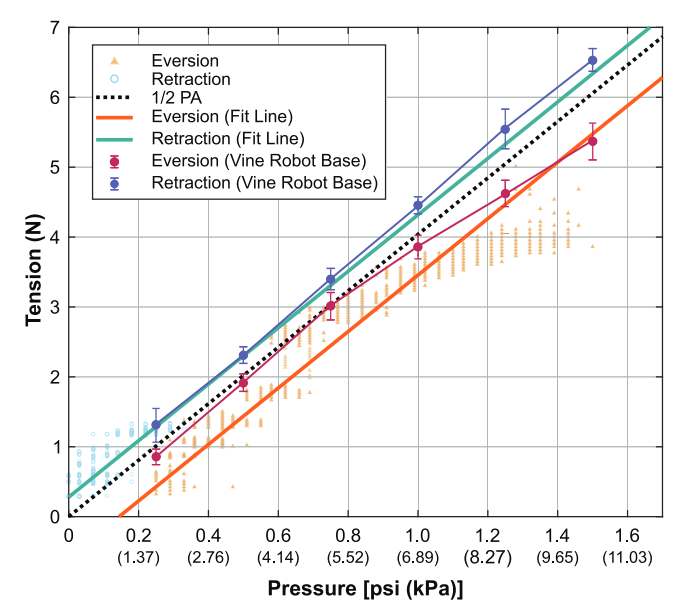


Fig. 6. Characterization of the relationship between Pressure P and Internal Tension  $F_T$ . The data corresponding to the Vine Robot Base provides a direct measure of  $F_o$ . With the data shown in Figure 5 corresponding to Pin 2 and Reel 2 (orange), we calculate  $F_o$ , found as the intercept of the fitted lines with the y-axis. There exist close agreement between direct measures and calculated values from other experimental measures. This indicates the pin behavior is well described by the spring force and the material eversion force losses.

nectors. The outer pins were designed to have pneumatic inputs on their sides, and the central pin had its input located at the bottom. The individual control of each soft growing pin was facilitated through the use of dedicated pressure regulators (QB3, ProportionAir). These regulators were controlled via an Arduino Mega microcontroller. A MATLAB graphical user interface (GUI) was designed to provide a user-friendly platform for altering pressure configurations, thereby streamlining the open-loop control of the entire array.

Figures 1 and 7 show the inflatable surface and its capabilities. The two distinct examples presented in Figure 7 exemplify the array's versatility. In the left example, a diagonal slant was generated, extending from a low extension in one corner to a higher extension in the opposing corner. Conversely, the right example demonstrated the simultaneous inflation of all pins in the array. Similarly, Figure 1 showcases grouped actuation of rows within the array. It is imperative to note that controlled retraction of the soft growing pins from one extension to a smaller one was found to be unfeasible due to the hysteresis in the spring retraction mechanism. Therefore, to transition between different surface configurations, the entire array was initially deflated before initiating a new surface actuation.

An additional set of pin combinations and movements was carried out (see supplementary video) to attain a comprehensive understanding of the array's capabilities. The resilience and compliance of the soft growing pins was demonstrated by their ability to withstand external forces such as human intervention. Additionally, the array was capable of immediate transitions between different surface configurations. Regarding individual actuation of pins, the repeatability of pressure actuation was tested by carrying out



Fig. 7. (Left) A diagonal slant surface can be transitioned to (Right) a flat, planar inflated surface. However, given the hysteresis in the retraction mechanism, the surface must transition first through the rest, deflated state (Center).

multiple cycles of inflation and deflation; each time, the input pressure achieved the same pin height.

While these demonstrations highlight the potential of soft growing pins for shape-changing inflatable displays, we discuss certain limitations inherent in the current design. First, the presence of hysteresis in the spring-actuated reels restricts smooth transitions between inflated surfaces. Secondly, despite the successful creation of different surfaces using open-loop control, it was observed that the pins exhibited slight variations in growth and retraction rates. This variability may be attributed to varied factors, such as pressure drops in the actuation lines, regulator irregularities, inconsistent reel fabrication, or variations due to processing speeds of the MATLAB GUI. Addressing these limitations will be imperative for the optimization of soft growing pins for future iterations of inflatable displays.

# VI. DISCUSSION

As demonstrated by the single and multi-pin experiments, the growing robot pressure driven eversion concept, when combined with a passive retraction mechanism, makes a high extension, compact option for pin displays.

The experimental results demonstrate that the relationship between input pressure, output length, and internal tension force can be modeled by expanding the mechanical model of growing robots to account for passive retraction. The pin behavior is accurately depicted by a combination of the material eversion force and spring force measured and calculated from our experiments. We observe that the eversion performance is in line with the expectations set by the model, as exhibited by the growth behavior (from direct and indirect measures) in Figure 6. The demonstrations in Section V show that even without closed-loop control, arrays of soft growing pins are capable of creating inflatable surfaces with a few iterations of pressure fine-tuning. Beginning from rest and given a desired inflated state, we can find a corresponding input pressure configuration (open-loop control) that will achieve said actuated state. Nevertheless, the experimental results suggest that retraction is a more intricate process to control. Consequently, we consider that, given some future redesign considerations, pin growth is controllable by pressure.

The pressure-extension characterization showed a large

hysteresis between growth and retraction; the spring force-extension experiment identified a sharp decrease in the spring force during retraction as the main cause of this observed hysteresis. For this reason, retraction can only occur when the pressure is reduced to a sufficiently low level. This hysteretic behavior restricts the control to extension of the pins. With the current spring actuated reel, it is impossible to retract directly from one length to another smaller height. Based on the experimental evidence, a spring-actuated reel with less hysteresis (or more linear elastic behavior) should enable controlled retraction from an extension to a smaller height by decreasing the input pressure accordingly without having to first bring the pin down to the un-pressurized, rest state.

Besides redesigning the spring-actuated reel to limit hysteresis, the passive retraction mechanism implemented in this initial prototype could potentially be replaced by an active one (likely in the form of a DC motor). However, the cost of a single growing pin unit would upsurge. We believe a passive retraction mechanism is ideal for our application, since adding just one row/column to an array of active-retraction pins would increase the cost drastically.

Despite the fact that our device has a high rate of expansion in relation to the size of the vessel, the maximum growth is restricted to only half of the length of the body that is contained within it. Even so, when compared to other growing pin developments, our eversion-growth prototype offers a more compact encasing of the growing body. We acknowledge that other growing pin technologies may be more adept at transitioning between heights. Nevertheless, a benefit of soft growing pins is that their growth is unlikely to be hindered by their environment. We believe that soft shape-changing interfaces have an advantage over rigid ones due to their flexibility and compliance to human touch. As humans are likely to interact with the pin arrays, our soft growing pins are designed to provide a safe physical experience.

#### VII. CONCLUSIONS AND FUTURE WORK

In this paper, we introduced a novel approach to augment human-machine communication by developing compact pneumatically actuated soft growing pins for inflatable haptic interfaces. We presented a detailed description of the pin's design and construction, including the use of cost-

effective components and the assembly process. Experimental characterizations of the pin's behavior demonstrated that the extension of the soft pin can be accurately modeled and controlled using pressure as the input. Moreover, our demonstrations showcased the feasibility of implementing individually actuated soft growing pins to create inflatable haptic surfaces, offering a promising avenue for shape-changing displays. However, it is important to acknowledge certain limitations. The presence of hysteresis in the spring-actuated reels restricts smooth transitions between inflated surfaces. Despite successful open-loop control of different configurations, variations in pin growth and retraction rates were observed, potentially due to various factors. Addressing these limitations is crucial for optimizing future iterations of inflatable displays using soft growing pins.

In summary, this research lays the foundation for innovative approaches to enhance human-machine communication and the development of shape-changing inflatable displays. Future work will focus on redesigning the spring-actuated reel to reduce hysteresis and enable full, closed-loop controlled extension and retraction. Additional future work will assess the usability and effectiveness of inflatable haptic interfaces through human user studies targeting practical applications. The potential to combine tactile stimulation with digital information in a spatial/physical environment opens up exciting possibilities for human-machine communication and immersive user experiences.

#### REFERENCES

- J. Alexander, A. Roudaut, J. Steimle, K. Hornbæk, M. Bruns Alonso, S. Follmer, and T. Merritt, "Grand challenges in shape-changing interface research," in *Proceedings of the 2018 CHI Conference on Human Factors in Computing Systems*, 2018, pp. 1–14.
- [2] S. Engert, K. Klamka, A. Peetz, and R. Dachselt, "STRAIDE: a research platform for shape-changing spatial displays based on actuated strings," in *Proceedings of the 2022 CHI Conference on Human Factors in Computing Systems*, 2022, pp. 1–16.
- [3] H. Hedayati, R. Suzuki, W. Rees, D. Leithinger, and D. Szafir, "Designing expandable-structure robots for human-robot interaction," Frontiers in Robotics and AI, vol. 9, p. 719639, 2022.
- [4] A. F. Siu, E. J. Gonzalez, S. Yuan, J. B. Ginsberg, and S. Follmer, "shapeShift: 2D spatial manipulation and self-actuation of tabletop shape displays for tangible and haptic interaction," in *Proceedings of the 2018 CHI Conference on Human Factors in Computing Systems*, 2018, pp. 1–13.
- [5] A. F. Siu, S. Kim, J. A. Miele, and S. Follmer, "shapeCAD: an accessible 3D modelling workflow for the blind and visually-impaired via 2.5D shape displays," in *Proceedings of the 21st International* ACM SIGACCESS Conference on Computers and Accessibility, 2019, pp. 342–354.
- [6] P. Schoessler, D. Windham, D. Leithinger, S. Follmer, and H. Ishii, "Kinetic Blocks: Actuated constructive assembly for interaction and display," in *Proceedings of the 28th Annual ACM Symposium on User Interface Software & Technology*, 2015, pp. 341–349.
- [7] K. Zhang, E. J. Gonzalez, J. Guo, and S. Follmer, "Design and analysis of high-resolution electrostatic adhesive brakes towards static refreshable 2.5 D tactile shape display," *IEEE Transactions on Haptics*, vol. 12, no. 4, pp. 470–482, 2019.
- [8] R. Suzuki, C. Zheng, Y. Kakehi, T. Yeh, E. Y.-L. Do, M. D. Gross, and D. Leithinger, "ShapeBots: Shape-changing swarm robots," in Proceedings of the 32nd Annual ACM Symposium on User Interface Software and Technology, 2019, pp. 493–505.
- [9] S. Je, H. Lim, K. Moon, S.-Y. Teng, J. Brooks, P. Lopes, and A. Bianchi, "Elevate: A walkable pin-array for large shape-changing terrains," in *Proceedings of the 2021 CHI Conference on Human Factors in Computing Systems*, 2021, pp. 1–11.

- [10] R. Suzuki, R. Nakayama, D. Liu, Y. Kakehi, M. D. Gross, and D. Leithinger, "LiftTiles: constructive building blocks for prototyping room-scale shape-changing interfaces," in *Proceedings of the* Fourteenth International Conference on Tangible, Embedded, and Embodied Interaction, 2020, pp. 143–151.
- [11] J. T. Gonzalez and S. E. Hudson, "Layer by Layer, patterned valves enable programmable soft surfaces." *Proceedings of the ACM on Interactive, Mobile, Wearable and Ubiquitous Technologies*, vol. 6, no. 1, pp. 12–1, 2022.
- [12] T. Morita, Z. Jiang, K. Aoyama, A. Minaminosono, Y. Kuwajima, N. Hosoya, S. Maeda, and Y. Kakehi, "InflatableMod: Untethered and reconfigurable inflatable modules for tabletop-sized pneumatic physical interfaces," in *Proceedings of the 2023 CHI Conference on Human Factors in Computing Systems*, 2023, pp. 1–15.
- [13] X. Wu, S.-H. Kim, H. Zhu, C.-H. Ji, and M. G. Allen, "A refreshable braille cell based on pneumatic microbubble actuators," *Journal of Microelectromechanical Systems*, vol. 21, no. 4, pp. 908–916, 2012.
- [14] Y. Hu, Z. Zhao, A. Vimal, and G. Hoffman, "Soft skin texture modulation for social robotics," in 2018 IEEE International Conference on Soft Robotics (RoboSoft). IEEE, 2018, pp. 182–187.
- [15] A. A. Stanley, J. C. Gwilliam, and A. M. Okamura, "Haptic jamming: A deformable geometry, variable stiffness tactile display using pneumatics and particle jamming," in 2013 World Haptics Conference (WHC). IEEE, 2013, pp. 25–30.
- [16] J. Pikul, S. Li, H. Bai, R. Hanlon, I. Cohen, and R. F. Shepherd, "Stretchable surfaces with programmable 3D texture morphing for synthetic camouflaging skins," *Science*, vol. 358, no. 6360, pp. 210– 214, 2017.
- [17] N. Baum and M. A. Minor, "Identification and control of a soft-robotic bladder towards impedance-style haptic terrain display," *IEEE Robotics and Automation Letters*, vol. 7, no. 4, pp. 12355–12362, 2022.
- [18] E. B. Sabinson and K. E. Green, "How do we feel? User perceptions of a soft robot surface for regulating human emotion in confined living spaces," in 2021 30th IEEE International Conference on Robot & Human Interactive Communication (RO-MAN). IEEE, 2021, pp. 1153–1158.
- [19] E. Sabinson, I. Pradhan, and K. Evan Green, "Plant-human embodied biofeedback (pheB): A soft robotic surface for emotion regulation in confined physical space," in *Proceedings of the Fifteenth International* Conference on Tangible, Embedded, and Embodied Interaction, 2021, pp. 1–14.
- [20] A. M. Rauf, J. S. Bernardo, and S. Follmer, "Electroadhesive auxetics as programmable layer jamming skins for formable crust shape displays," in 2023 IEEE International Conference on Robotics and Automation (ICRA). IEEE, 2023, pp. 2591–2597.
- [21] R. Suzuki, E. Ofek, M. Sinclair, D. Leithinger, and M. Gonzalez-Franco, "HapticBots: Distributed encountered-type haptics for VR with multiple shape-changing mobile robots," in *The 34th Annual ACM Symposium on User Interface Software and Technology*, 2021, pp. 1269–1281.
- [22] Z. M. Hammond, N. S. Usevitch, E. W. Hawkes, and S. Follmer, "Pneumatic Reel Actuator: Design, modeling, and implementation," in 2017 IEEE International Conference on Robotics and Automation (ICRA). IEEE, 2017, pp. 626–633.
- [23] E. W. Hawkes, L. H. Blumenschein, J. D. Greer, and A. M. Okamura, "A soft robot that navigates its environment through growth," *Science Robotics*, vol. 2, no. 8, p. eaan3028, 2017.
- [24] L. H. Blumenschein, A. M. Okamura, and E. W. Hawkes, "Modeling of bioinspired apical extension in a soft robot," in *Conference on Biomimetic and Biohybrid Systems*. Springer, 2017, pp. 522–531.
- [25] L. H. Blumenschein, M. M. Coad, D. A. Haggerty, A. M. Okamura, and E. W. Hawkes, "Design, modeling, control, and application of everting vine robots," *Frontiers in Robotics and AI*, vol. 7, p. 548266, 2020
- [26] M. M. Coad, R. P. Thomasson, L. H. Blumenschein, N. S. Usevitch, E. W. Hawkes, and A. M. Okamura, "Retraction of soft growing robots without buckling," *IEEE Robotics and Automation Letters*, vol. 5, no. 2, pp. 2115–2122, 2020.
- [27] M. M. Coad, L. H. Blumenschein, S. Cutler, J. A. R. Zepeda, N. D. Naclerio, H. El-Hussieny, U. Mehmood, J.-H. Ryu, E. W. Hawkes, and A. M. Okamura, "Vine robots," *IEEE Robotics & Automation Magazine*, vol. 27, no. 3, pp. 120–132, 2019.